In Vivo Thermography-Based Image for Early Detection of Breast Cancer Using Two-Tier Segmentation Algorithm and Artificial Neural Network

Asnida Abd Wahab, Maheza Irna Mohamad Salim and Maizatul Nadwa Che Aziz

Abstract Breast cancer is the most common form of cancer among women globally. Detecting a tumor at its early stages is very crucial for a higher possibility of successful treatment. Cancerous cells have high metabolic rate which generate more heat compared to healthy tissue and will be transferred to the skin surface. Thermography technique has distinguished itself as an adjunctive imaging modality to the current gold standard mammography approach due to its capability in measuring the heat radiated from the skin surface for early detection of breast cancer. It provides an additional set of functional information, describing the physiological changes of the underlying thermal and vascular properties of the tissues. However, the thermography technique is shown to be highly dependent on the trained analyst for image interpretation and most of the analyses were conducted qualitatively. Therefore, the current ability of this technique is still limited especially for massive screening activity. This chapter presented a proposed technical framework for automatic segmentation and classification of abnormality on multiple in vivo thermography-based images. A new two-tier automatic segmentation algorithm was developed using a series of thermography screening conducted on both pathological and healthy Sprague-Dawley rats. Features extracted show that the mean values for temperature standard deviation and pixel intensity of the abnormal thermal images are distinctively higher when compared to normal thermal images. For classification, Artificial Neural Network system was developed and produced a validation accuracy performance of 92.5% for thermal image

A.A. Wahab (✉) · M.I.M. Salim · M.N.C. Aziz
Faculty of Biosciences and Medical Engineering, Universiti Teknologi Malaysia, V01 Satellite Building, Skudai, Johor, Malaysia
e-mail: asnida@biomedical.utm.my

M.I.M. Salim
e-mail: maheza@biomedical.utm.my

M.N.C. Aziz
e-mail: nadwaaziz@gmail.com

E.Y.K. Ng and M. Etehadtavakol (eds.), *Application of Infrared to Biomedical Sciences*, Series in BioEngineering,
DOI 10.1007/978-981-10-3147-2_8

abnormality detection. In conclusion, this study has successfully demonstrated that for massive or routine screening activities, the proposed technical framework could provide a highly reliable clinical decision support to the clinicians in making a diagnosis based on the medical thermal images.

Keywords Thermography · Thermal image processing · Artificial neural network

1 Introduction

Breast cancer is the most common cancer experienced among women globally [1, 2]. The number of breast cancer incidences has steadily increased, and breast cancer has recently appeared to be the second leading cause of death in women [3]. National Cancer Institute of Canada has estimated that two out of five women will develop breast cancer during their lifetime, and approximately one out of four will die as a result of this disease [2]. Although breast cancer is highly treatable if it is detected at the early stages, the number of women diagnosed with breast cancer is at the later stage especially those in developing and third world countries due to the unavailability of portable breast imaging facilities and lack of awareness [4, 5].

Mammography technique is the current gold standard morphological-based imaging tool that is used in clinical practices globally. However, this technique exhibits low sensitivity in dense breast tissue composition or in young women. Additionally, it requires breast compression during screening and exposes to harmful radiation [6–9]. On the other hand, infrared thermography technique has shown to be a potential adjunctive tool for detecting breast cancer [10–12]. Previous studies show that the heat generated by cancerous cells due to the high metabolic rate will be transferred to the skin surface via heat conduction and heat convection through both tissue and blood vessel respectively. Infrared thermography will then measures the heat radiation emitted from the skin surface and converts it into a visual thermal image format with its respective temperature values [8, 13]. It is a non-invasive and effective alternative modality for early detection of breast cancer with simple screening procedure requirement, high accuracy for surface temperature measurement, low in cost and available in small sizes which allow mobility for bigger population coverage [10, 11, 14, 15].

With the advances in the infrared camera technology and computerized image processing system, the subtle alteration of temperature associated with underlying physiological changes is becoming more accessible in thermography, enabling high accuracy thermal-based breast cancer detection. However, this technique is highly dependent on trained analysts for thermal image interpretation which means, a single thermal image may be interpreted differently by different analysts relative to their respective skills, experiences, and health conditions [16, 17]. As a result, the clinical applicability of the thermography technique is still limited, and it is very crucial to further improve the technical aspects to increase the overall system reliability for high acceptance into a clinical practice.

Unlike any other applications of thermography (e.g., image from surveillance camera) which mainly focus on the presence of overall subject, thermal images obtained from medical thermography present a different temperature patterns and contours related to the underlying physiological changes which occur at a specific area within the subject. Thus, detecting and segmenting the symptomatic region from the rest could be a very challenging task due to the inhomogeneous nature and lack of clear limits in each subject. In addition, different camera settings and initialization that could vary the size of subject in each frame. As a consequence, most researchers prefer to manually segment or to use a semi-automatic region of interest (ROI) segmentation method for further measurement and analysis.

In the case of qualitative breast cancer diagnosis, the ROI segmented must include both breasts since clusters of lymph nodes are found in the axillar region, above the collarbone and chest. Herry and Frize have developed a contour detector using morphological operators, as a means of comparing the intensity distribution between both breasts. However, the initial segmentation of the subject has been carried out manually [18]. Lipari and Head have constructed a semi-automatic segmentation method, wherein each breast was divided into four distinct quadrants, and an asymmetrical pattern between the quadrants was used for further. But, lack of ideal body symmetry in the images has resulted in missing data for comparison [14]. Another semi-automatic segmentation has been proposed by Scales and others which comprised of eight different steps. They have reported that only 4 out of 21 images result in satisfactory ROI detection and errors were due to detection of inframammary fold and bad edge detection [19]. However, for large number of thermal images that need to be processed, both semi-automatic and manual segmentation will be time consuming with a high chance of result inconsistency due to fatigue. Motta and others have recently developed a fully automatic segmentation method based on automatic threshold and border detection, and extraction of infra mammary folds. They have used mathematical morphology and cubic spline interpolation to separate both breasts symmetrically. However, the ROI detected may exclude the portion of upper quadrant of the breast [20]. Therefore, most of the researchers are currently focusing on developing an autonomous method for breast segmentation.

Contrarily, in quantitative analysis, important features required to be extracted from the ROI and to be fed into a classification system for diagnosis purposes. In this particular case, the presence of breast images for processing is not necessary but accurate ROI detected is crucial in order to ensure that features extracted from the thermal images are highly reliable. In Schaefer and others' studies, the ROIs were segmented manually by an expert before fuzzy rule-based classification system was applied [21, 22]. On the other hand, Ng and Kee have performed manual segmentation on patients' thermal images prior feeding them in an advanced integrated breast thermography classification method [23]. However, fully automatic ROI segmentation is still preferred to reduce overall computational time and intervention by analysts especially when dealing with numerous thermal images.

Although infrared thermography has not yet been applied to clinical practice, this technique otherwise has shown to be an ideal modality for an upfront and routine breast screening due to its passive nature and simple screening procedure [10, 11]. However, a reliable classification of thermal image abnormalities would be a steadfast indicator for further assessment using other sophisticated imaging techniques. Therefore, this chapter proposed a new technical framework for thermal image computer-aided diagnosis which integrates automatic segmentation, feature extraction using both characteristics from visual and temperature data for image abnormality classification. The main focus is to assist the clinicians in analysing multiple thermal images accurately with minimal intervention and storage requirement for mass screening activities.

A process of selecting different features from both visual image (pixel based) and data temperature (temperature point) is compulsory in order to compose a feature vector for classification between abnormal and normal thermal images [24]. However, due to storage limitation, most researchers have chosen to process and extract the pixel related features available on the thermal images. Acharya and others have measured smoothness, coarseness and regularity of pixels from thermal images in order to further segregate these textures into two main classes, namely structural and statistical. Later, they have used support vector machine (SVM) method for classification [25]. Schaefer and others have extracted basic statistical features, histogram features, cross co-occurrence matrices and mutual information from the thermal images [21, 26]. In addition, Kuruganti and Qi have extracted features such as mean, variance, kurtosis, peak pixel intensity and entropy, in order to validate their proposed classification method [27]. Jakubowska and others have extracted four different image features based on histogram, co-occurrence matrix, gradient and run-length matrix. They have then utilized artificial neural network (ANN) method for classification. Nevertheless, extracting and analyzing the features from the pixel-based aspect alone for classification might introduce asynchronization of data especially when extensive preprocessing technique is carried out [28]. Therefore, Ng and Kee have extracted thermal information from the data temperature point with additional history information, to determine breast abnormalities [23]. Borchartt and others have considered features including range of temperature, mean temperature, and standard deviation of temperature in their study and used SVM to evaluate the selected features [29]. Both studies have achieved a high accuracy performance of 80.95 and 85.71% respectively.

It can be seen that different combinations and flows of image processing methods have been applied and proposed previously, in accordance with the specific objectives of each study. In general, the image segmentation and feature analysis techniques have been developed from a simple single method analysis to an advanced integration analysis techniques depending on the different objectives that need to be achieved and also the availability of image data types.

2 Data Collection

2.1 Animal Preparation

The use of animals in this study was approved by the institutional review board of the Universiti Kebangsaan Malaysia, Animal Ethics Committee (UKMAEC), Selangor Malaysia. Two groups of female Sprague-Dawley strain rats consisting of fifteen pathological (abnormal) rats and fifteen control (normal) rats weighing between 180 and 250 g were housed in polypropylene cages with wood shavings used as bedding at an ambient room temperature, as well as access to water and food ad libitum with a 12 h light/dark cycle. For pathological group, a single dose of 10 mg of 7, 12-dimethylbenz(α)anthracene (DMBA), a carcinogenic chemical used widely to produce mammary tumor, was dissolved in 0.5 mL of sesame oil purchased from Sigma-Aldrich and administered via a subcutaneous injection into the rats at the average age of 57 days [30]. All rats were palpated weekly to detect the presence of mammary tumors. The induced rats were then allowed to adapt to a new environment for two weeks before thermography screenings were carried out.

2.2 In Vivo Thermography Screening

The entire experiment has been conducted in a small preparation room with minimal light exposure located in the Clinical Animal Laboratory of the Faculty of Bioscience and Medical Engineering (FBME) at the Universiti Teknologi Malaysia (UTM) in Johor, Malaysia. The room temperature was controlled and maintained at a range of 20–22 °C, using an air-conditioning system with relative humidity of 60–65%. The fluorescent lights available in the room were turned off during acclimatization and screening processes [31]. This will ensure factors such as high variations in room temperature, different percentages of light exposure, and other possible factors that could influence the result in a significant way were minimized. With this approach, a higher result consistency could be achieved. The images were acquired using an Epidermal Thermal Imaging Professional (ETIP) infrared imaging camera system model 7640 P-Series, manufactured by Infrared Camera Incorporation, Texas USA, with a resolution of 640 × 480 pixel, and a field of view of 49°/18 mm × 36°/25 mm, using a focal plane array microbolometer type detector, a spectral range of 7–14 µm, a thermal sensitivity of 0.038 °C with a temperature range of −40 to 400 °C and an accuracy of ±1% of readings.

The camera was mounted on a flexible arm which was connected to the display monitor as shown in Fig. 1. The distance between the camera to the sample was manually controlled, in order to get the best display output. The initialization of the camera was carried out once prior to screening, in order to reduce noise and stabilize the system.

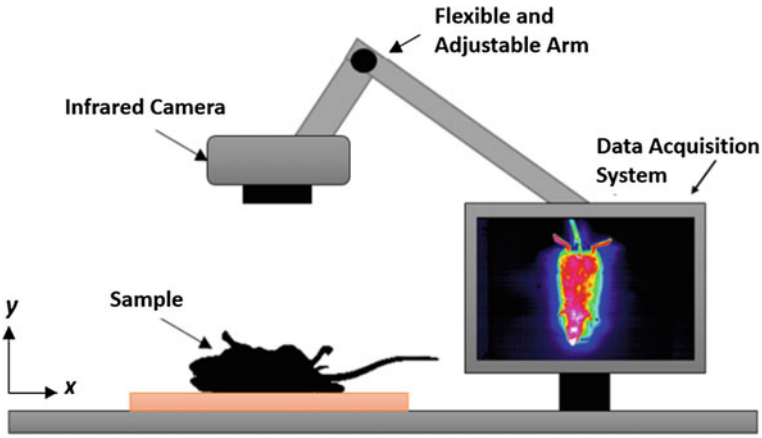

Fig. 1 In vivo thermography screening setup

All rats were allowed to acclimate to the room temperature of range from 20 to 22 °C for up to 15 min before screening. Since a still or minimal movement target is required during the screening process, a single dose of 0.1 ml/100 g of Ketamine–Zoletil–Xylazine (KTX) anesthetics combination was administered into each rat via an intramuscular route to provide a light anesthesia for 30–45 min [32]. A polyethylene decapicone restrainer was used for handling and approaching the rats. Anesthetized rats were placed back in their individual cage until they were fully unconscious. The rats were weighed and palpated to check for any lumps or tumor multiplicity as shown in Fig. 2 before the screening and all this data was measured and recorded accordingly.

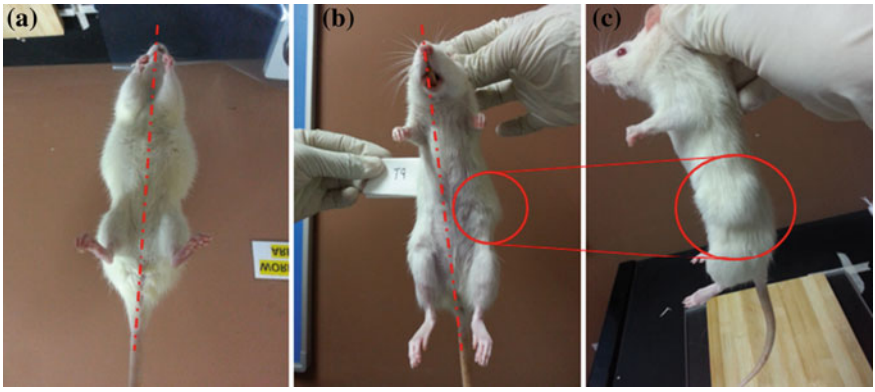

Fig. 2 Frontal view of **a** a normal rat with symmetrical body shape, **b** a pathological rat with palpated lump on the left side of the body and **c** side view of a pathological rat with palpated lump

Rats were then placed on the wooden plate in anterior position facing the camera for ten minutes. Images were captured at a rate of five frames per minute and thermal image in the *joint photographic expert group* (jpeg) format and temperature data point in the *comma separated values* (csv) file formats were stored for further analysis and processing. All screened rats were kept in their individual cages, and were monitored hourly for any post-procedure effects.

2.3 Disease Verification

After 12 weeks of consecutive screening, histology test and disease verification procedure were carried out to ensure that the symptomatic hotspot areas detected on the thermal images were due to the cancer disease and not any other pathologies. All surviving rats were euthanized by using drug overdose method to harvest the breast tissue sample. Before excision, the fur around the breast area was shaven and tissue samples were cut into smaller pieces and immersed inside 10% buffered formalin solution for fixation and preservation purposes. The tissue were processed, embedded in paraffin and section at 5 μm. The sections were then mounted on the

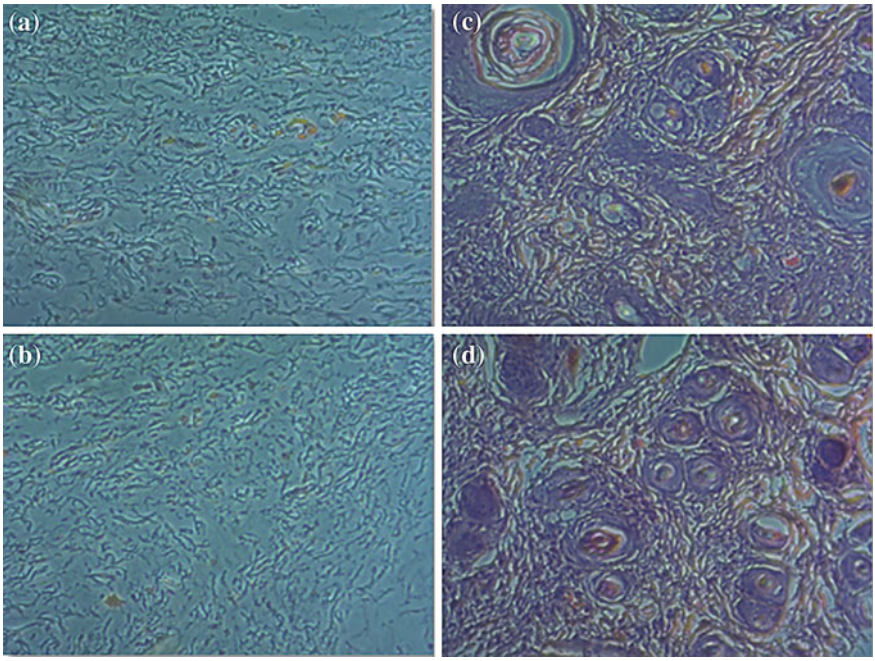

Fig. 3 Histological view of **a**–**b** cell arrangement in healthy breast tissue and **c**–**d** cell arrangement in cancerous tissue

glass slides and stained with haematoxylin and eosin to give contract to the tissue as well as to visualize the microscopic structures.

An expert from Pathology and Clinical Laboratory, Johor, Malaysia has classified both normal and pathological samples based on gross morphologic appearance of the tissue as shown in Fig. 3. Obtained histology results have confirmed that all specimens within the pathological group had high grade invasive ductal carcinoma of the mammary gland, with the presence of the syringomatous carcinoma component in certain samples, while healthy group specimens were confirmed to be normal without the presence of any cancerous cells.

3 Image Processing

A two-tier segmentation algorithm was developed in order to detect the symptomatic regions on the visual image and mapped them to the corresponding temperature data file for feature extraction and classification purposes. This will assist the clinician in diagnosing the thermal image by focusing only on the data extracted from affected area and not having to examine the whole image captured.

3.1 First Tier: Segmentation for Subject of Interest (SOI)

The first segmentation process involved separating the subject from the background in the thermal images using histogram based separation method. This eliminates the possibility of the system to detect any hot spot area in the background as one of the possible symptomatic region of interest since each pixel in the visual image corresponding one temperature value. Two vertical points namely x_1, y_1 and x_2, y_2 need to be chosen by the analyst once during system initialization, in order to approximately mark the subject position based on laboratory setting as shown in Fig. 4.

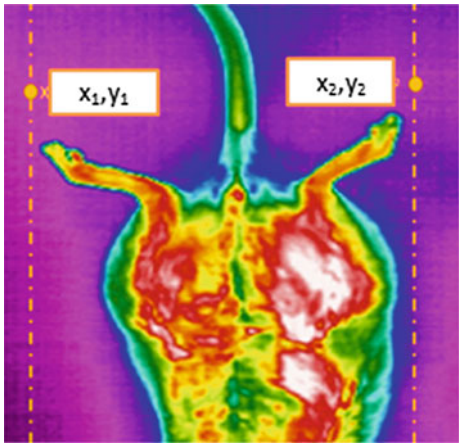

Fig. 4 Example of selection of two vertical points

Local information such as the overall intensity and vertical profile based on the selected vertical points were utilized in order to perform an individual image background correction. This particular step will allow flexibility alteration to different types of room and equipment settings including distance of the subject to the camera, the zooming function and the various physical sizes of the subjects.

Figure 5 shows a flowchart of new algorithms proposed for SOI segmentation. The raw image obtained from the thermography screening was preprocessed. Since different system have different color schemes (e.g., RGB, thermal, rainbow), analyst has to select one channel that suit the system best during initialization phase. The calculation of the mean intensity (μ_i) value as shown in Eq. 1 was used to generate a new matrix layout mapping with identical intensity value.

$$\mu_i = \frac{1}{N}\sum_{i=1}^{N} x_i \tag{1}$$

where N is the total pixel determined using vertical range (0—y_1 and y_2—max vertical pixel number) and x_i is the intensity value of each pixel measured.

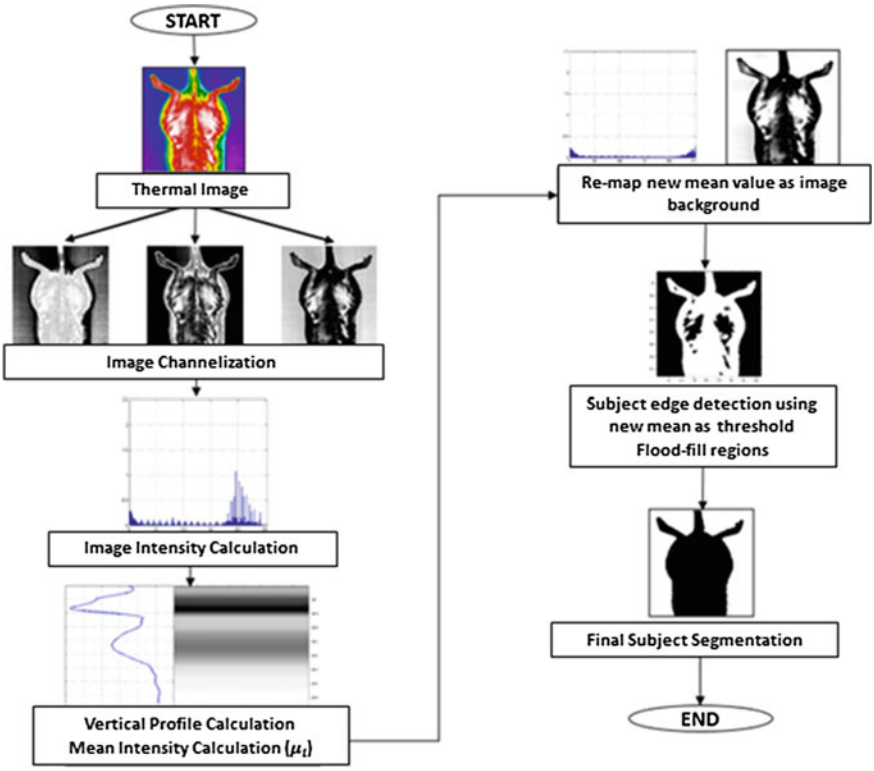

Fig. 5 Flowchart for SOI segmentation

Each pixel value in the output image, $I'_{(i,j)}$, was generated by the subtraction of the mean intensity value from the pixel value in the input image, $I_{(i,j)}$, as shown in Eq. 2.

$$I'_{(i,j)} = I_{(i,j)} - \mu_i \tag{2}$$

Next, the image was converted into a binary format background and was remapped onto a new image. Subject edge detection was performed within the subject with a flood-fill operation applied in order to eliminate any brightness discontinuity and to allow only one subject boundary to be detected. For performance evaluation, a comparative study between the proposed algorithm and the conventional segmentation methods namely the Otsu and Active Contours was performed.

3.2 First Tier: Result and Discussion

Figure 6 shows the output of the SOI segmentation carried out on multiple thermal images using the newly developed algorithm. It can be seen that although each thermal image has a different image background profile, the proposed algorithm is capable of detecting the SOI accurately, while manual segmentation requires longer time due to the complicated subject outline.

On the other hand, Fig. 7 shows the segmented image using Otsu's method. It can be clearly observed that the segmented image did not show any distinct boundary between the subject and the background. This is due to the default thresholding applied in Otsu's method which is not suitable for use in thermal

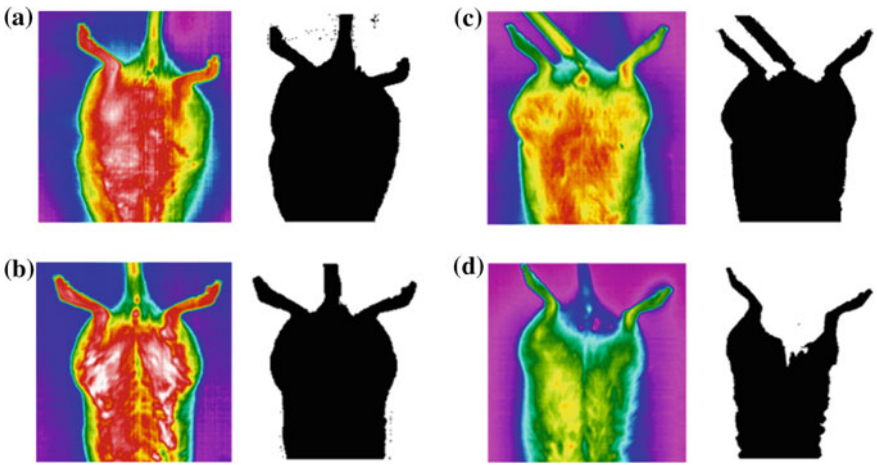

Fig. 6 Segmentation of multiple thermal images using a new developed algorithm

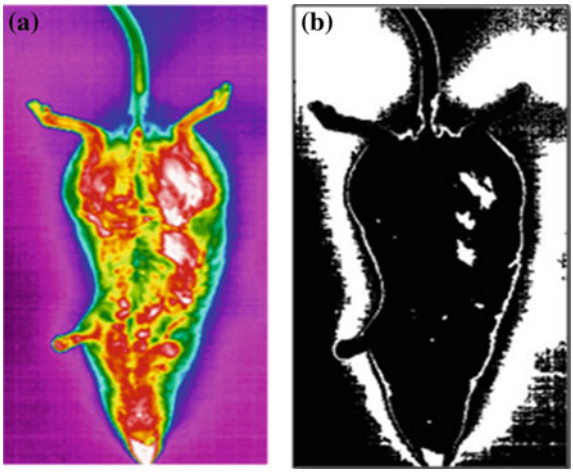

Fig. 7 Thermal image segmentation using Otsu's method

images due to its inhomogeneous color contours. However, for images with homogeneous objects and backgrounds Otsu's method has been shown to be very precise.

Figure 8 shows the segmented thermal image, using the Active Contour method with a different iteration number used. Interestingly, it can be observed that the higher the iteration, the detected edge becomes smoother and clearer. However, the disadvantage of larger iteration numbers is that they require higher computational loads and longer times to process. In addition, for the large number of images which need to be processed, single settings on iteration number may not be suitable to be used and could result in subject segmentation inconsistency.

Further morphological and quantitative comparisons were made based on the edge detection line drawn on each SOI segmented image and time taken for each segmentation as shown in Fig. 9 and Table 1 separately. It was observed that the

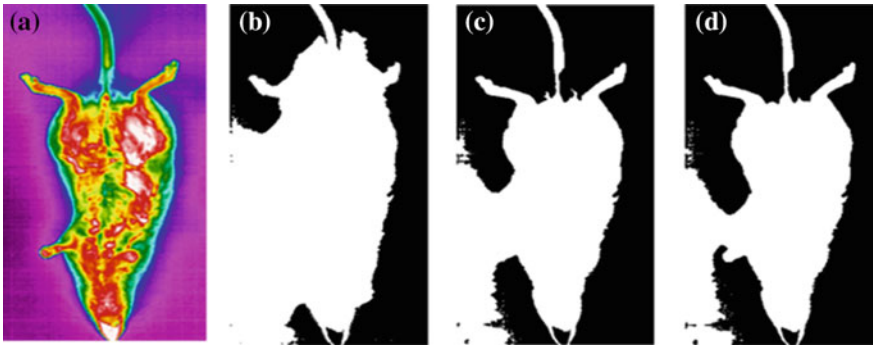

Fig. 8 Thermal image segmentation using the Active Contour method including **a** the raw thermal image **b** after 300 iterations **c** after 600 iterations and **d** after 700 iterations

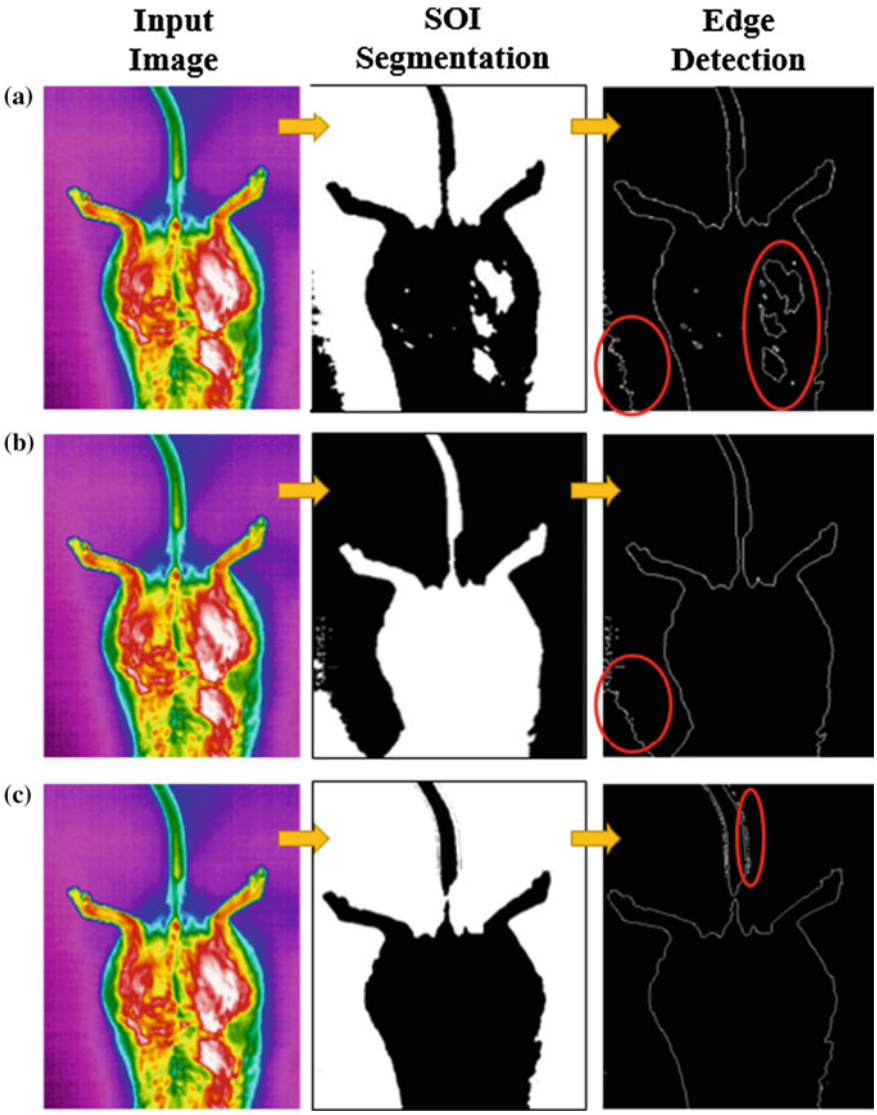

Fig. 9 Comparison of segmentation methods using **a** the Otsu's method **b** the Active Contour with 700 iterations and **c** the newly proposed SOI algorithm

Table 1 Processing time comparison

Method	Time (mean ± std) (s)
SOI segmentation	0.6415 ± 0.0429
Otsu's method	0.7130 ± 0.0651
Active Contour (700)	30.318 ± 1.0519

newly proposed SOI segmentation algorithm has outperformed the existing methods in both aspects, producing a distinguished boundary line between SOI and clear image background with lowest processing time. However, since initial image cropping can be controlled, analyst may choose to exclude the lower part of the body to minimize the undesirable noise captured along the tail. In previous clinical case study, areas such as face, neck and lower body were excluded during image processing. A corrected background profile shows a smooth and consistent pixel arrangement.

Segmented SOI from Otsu's method is shown to be the least accurate with a comparable processing time to the newly developed algorithm. The thermal image output was shown to capture the largest amount of background information. This may reduce the ROI segmentation accuracy in the later stage. Likewise, the background profile displayed a polluted pixel arrangement. Otsu's method has a drawback as it uses a single parameter setting, although this method is generally preferred in other digital image processing field, it seems to be not suitable for SOI segmentation in medical thermal image processing.

Contrariwise, the Active Contour method with 700 iterations produced a better cut-off line between the subject and background than Otsu's method with a small background area captured, but this method requires the longest processing time and highest load among others.

Therefore, the newly proposed SOI segmentation algorithm has proven to be capable for segmenting the SOI in different thermal images automatically with high accuracy and requires less processing load and time.

3.3 Second Tier: Segmentation for Region of Interest (ROI)

The second-tier segmentation algorithm was developed to detect the possible ROIs within the subject, where any presence of hotspots outside the SOI boundary will be disregarded in this stage.

Figure 10 shows the overall flow chart for the ROI segmentation process. By using the mean intensity value calculated previously in the SOI segmentation stage as a new threshold, all possible ROIs could be determined. Equation 3 shows the possible ROIs selection criteria where value '1' represents positive possible ROIs and value '0' represent non-ROI hotspots.

$$R_{\text{poss}} = \begin{cases} 1 & \text{if } R_i > \mu_i \\ 0 & \text{otherwise} \end{cases} \quad (i = 1, 2, 3 \ldots n), \tag{3}$$

where R_{poss} are the possible regions which have pixel value larger than the mean value and R_i are all hot spot in the SOI segmented. Figure 11 shows the output of possible regions detected within the subject using two different regions selection schemes.

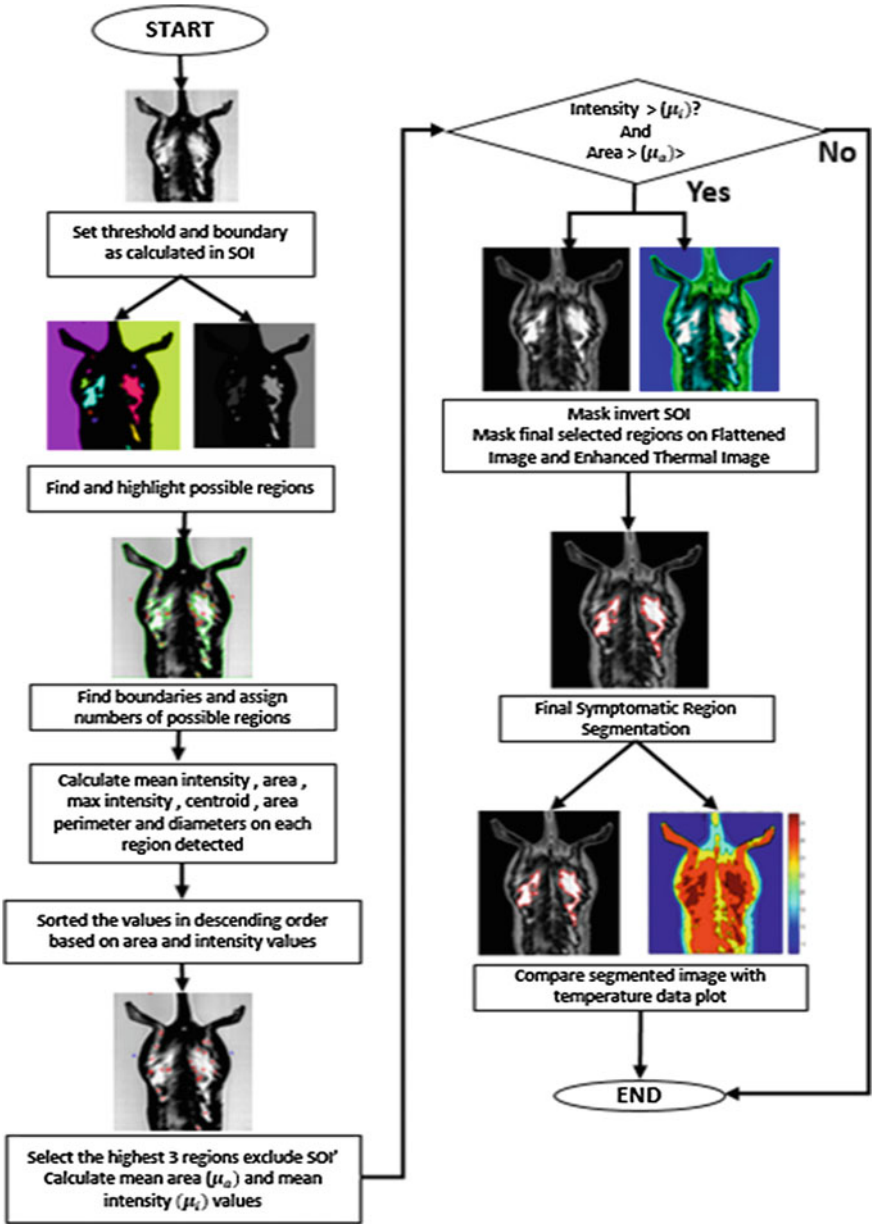

Fig. 10 Flowchart for ROI segmentation

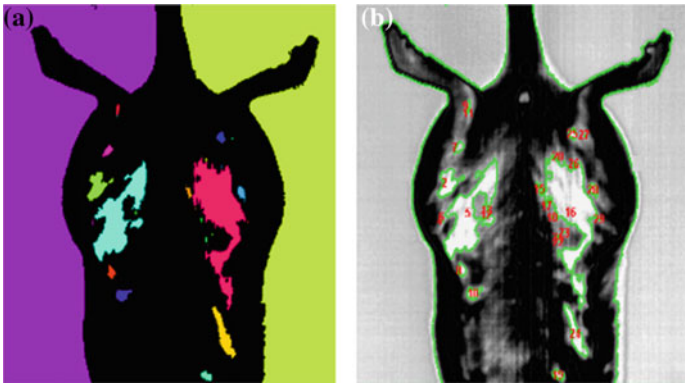

Fig. 11 Example of possible hotspot regions detected with **a** color highlighted and **b** numbered

Local parameter properties, such as the intensity, centroid value, diameter and area of each identified region were measured and tabulated for all possible symptomatic ROIs. Two parameters namely mean area (μ_a) and mean intensity (μ_i) were calculated and used to determine the final ROIs (R_{final}) selection as shown in Eq. 4.

$$R_{\text{final}} = R_{\text{poss}} > (\mu_a \cap \mu_i) \tag{4}$$

Mean area was used to eliminate the presence of smaller hotspots which are insignificant, while mean intensity was used to eliminate low temperature areas. Areas which satisfied both criterions were masked on the SOI segmented thermal image. Regions that not belong to these criterions were ignored, and if there were none detected, the image is considered normal and the algorithm will be terminated.

Finally, the output result of the ROI segmented image was compared to the temperature data contour plot, in order to validate and verify whether the final ROIs detected from the thermal image are in the same position as those generated from the raw temperature data file. This is a very important step as processing a raw temperate data file in the '*comma separated value*' or csv format can significantly increase the processing load requirement by thrice. However, qualitative comparison alone is insufficient to evaluate the performance of the developed ROI segmentation method. Hence, four different area based evaluation methods namely Dice Similarity Coefficient (DSC), Jaccard Index (JI), Relative Area Different (RAD) and Area Overlap Error (AOE) were used to analyze and compare ROI obtained via automated segmentation and using manual tracing for all samples [33–35].

DSC identifies the degree of area that is overlapping between automated and manual segmentation. On the other hand, Jaccard Index study the ratio of area in common of both automated and manual segmentation methods. RAD calculates the difference between area of the automated segmentation and the one from manual tracing where negative values indicate that the region segmented by the proposed

method is smaller than that by manual tracing. Positive values indicate that the region segmented manually is smaller than the one segmented by the system. AOE, which is based on JI, shows that ratio of the area that is not intersecting between both regions.

Hence, segmenting the ROI in its visual format and extracting features based on the ROI mapped onto the temperature data file will certainly increase the overall processing efficiency.

3.4 Second Tier: Results and Discussion

Figures 12 and 13 show the results of ROI segmented in both normal and abnormal thermal images respectively.

It was observed that for normal thermal image, no symptomatic region was detected and mapped onto the SOI segmented image. However, for the abnormal thermal image, few distinctive symptomatic regions were detected and mapped onto the SOI segmented image. Although a large hotspot could be seen clearly on the raw thermal image, only areas which satisfied the criterion set earlier were selected. This is crucial to guide and assist the clinicians in diagnosing a patient. As visual image only carries pixel information, it is important to ensure that ROI segmented corresponded to the highest temperature on the raw thermal image.

Based on the output result obtained in Fig. 14a, it is clearly shown that the ROIs detected have correspondingly matched their respective temperature data shown in Fig. 14b, c. In addition, an automated segmentation method developed shown to have high similarity coefficient to manual tracing with 97.38 and 94.89% for both DSC and JI respectively as shown in Table 2. RAD shows a positive value of 5.38 which indicates that bigger region segmented using manual tracing than the one segmented automatically. This is due to the small temperature changes along the border of symptomatic regions that was not able to be differentiated visually.

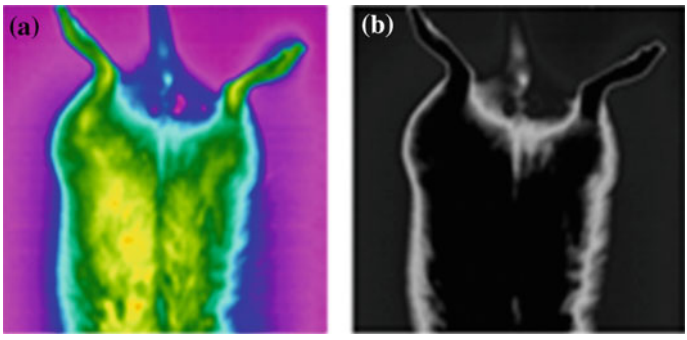

Fig. 12 ROI segmentation of normal thermal image **a** raw thermal image, and **b** ROI masked on raw image

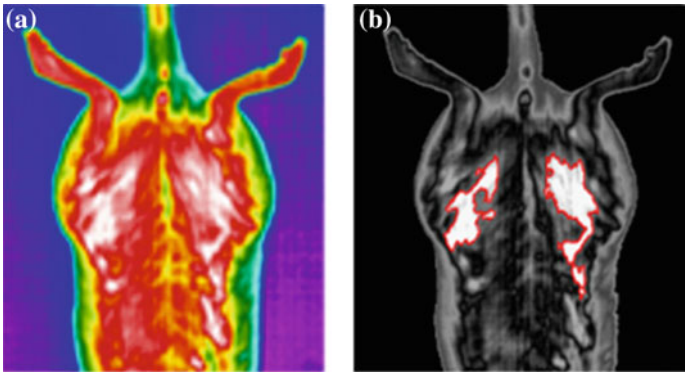

Fig. 13 ROI segmentation of abnormal thermal image **a** raw thermal image, and **b** ROI masked on raw image

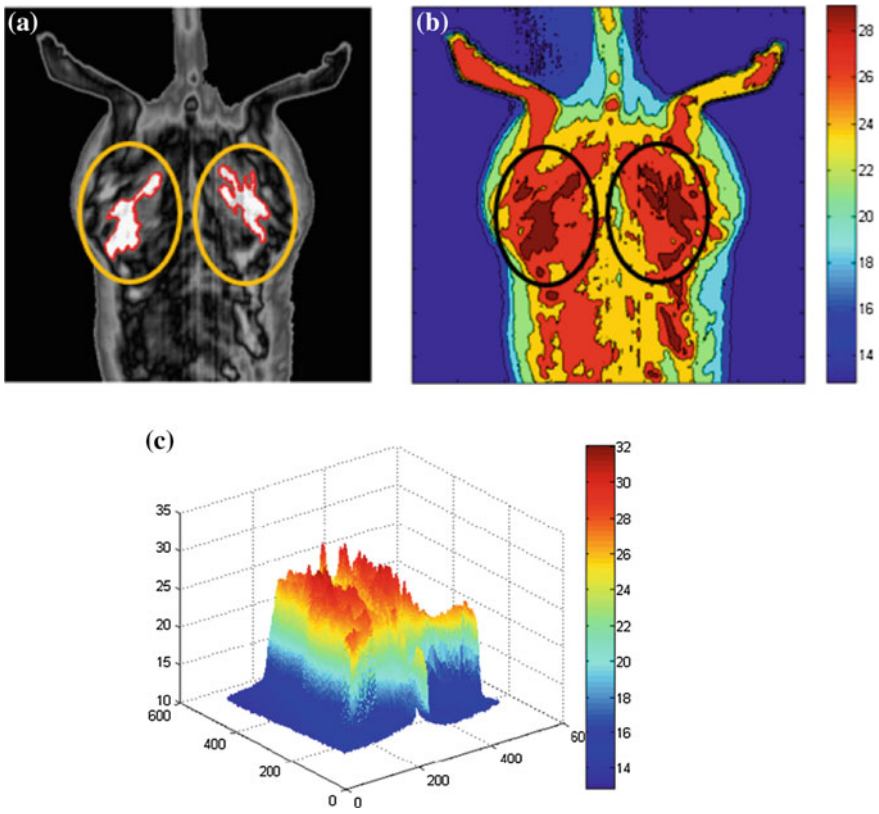

Fig. 14 Comparative analysis between **a** ROI segmented thermal image and **b**, **c** temperature data plot in 2D and 3D respectively

Table 2 Quantitative performance measurement between automated and manual segmentation

Dice similarity coefficient (%)	Jaccard index (%)	Relative area difference (%)	Area overlap error (%)
97.38	94.89	5.38	5.10

Finally, AOE result obtained shows that there was a high resemblance between both regions segmented using manual and automated methods.

4 Automatic Abnormalities Detection

Once the final ROIs were detected, the pixel number lies within the ROI boundary will be used as a reference to extract the temperature related information from the temperature data file. For normal thermal images with no ROI boundary detected, temperature information within an area of size 50 × 50 pixels from the subject midpoint were extracted. Five different features including mean intensity, mean temperature, maximum temperature, minimum temperature and standard deviation were extracted. These data which were taken from a total of 200 sets of thermal images and were then sampled into three different categories namely training, testing, and validation. Target value of '1' was assigned to all pathological images and target value '0' was assigned to all thermal images captured on normal samples. In this study, an artificial neural network (ANN), a widely used classification method in medical diagnosis has been utilized to classify whether the thermal image is belong to the abnormal group or otherwise [36, 37]. ANN processes the data in parallel distributed mainframe and has the ability to learn on the basis of the input data they fed. The network was first trained using back propagation algorithm which employs steepest gradient descent with momentum and consists of one input layer, two hidden layers and one output layer with sigmoid and linear transfer function were applied in the hidden layers. The network was then optimized to reduce over fitting before data testing and validation can be performed by varying the training parameters including number of neuron, learning rate, momentum constant, and iteration rate. The values of each parameter was considered optimum when the network produces the lower mean squared error (MSE) value with high prediction accuracy performance. The prediction values obtained from both testing and validation steps were further evaluated for group recognition and accuracy measurement. The MSE calculation is shown is Eq. 5.

$$E_k = \frac{1}{2}\sum_{j=1}^{N}\left(T_{kj} - O_{kj}\right)^2, \tag{5}$$

where E_k is the MSE value, T_{kj} represent target value for jth output neuron, O_{kj} is the actual output and N is the total output number of neuron. The range used for

both groups are shown in Eqs. 6 and 7. While the accuracy calculation was made based on conditions in Eq. 8.

$$-0.2 < \text{Pnormal} < 0.2 \tag{6}$$

$$0.8 < \text{Pabnormal} < 1.2 \tag{7}$$

$$\text{Accuracy } (\%) = \frac{\text{Total of Correct Detection}}{\text{Total Detection}} \times 100 \tag{8}$$

4.1 Features Extraction and Classification

Figure 15 shows the comparison of temperature and mean intensity values for all features extracted including maximum temperature, minimum temperature, mean temperature and standard deviation from data temperature file and mean intensity values from thermal image for both normal and pathological rats separately. The temperature standard deviation and mean intensity values for both groups were shown to be the most significant distinguishable features among others. Mean values (°C) of 0.433 ± 0.1547 and 0.109 ± 0.037 for both the abnormal and normal groups were observed in temperature standard deviation while distinctive values of 216.9417 ± 8.6471 and 167.0467 ± 3.708 were obtained in pixel mean intensity.

Maximum temperature and mean temperature showed a comparably significant difference with minimal correlation, while the minimum temperature was observed to have the least significant difference where values from the third quartile (Q3) of a normal group could be mistakenly assigned to the abnormal group. Data which have outlier values were excluded for classification. Nonetheless, these features have been considered with additional selected features from image processing to be used in the development of ANN as they fulfil the least requirements needed for robust prediction.

For classification, a total of 120 sets of data (60 normal and 60 abnormal images) were used in the training process, 40 sets of data (20 normal and 20 abnormal images) for testing and another 40 sets of data (20 normal and 20 abnormal images) were used for validation purposes. A final optimized network architecture consists of 5 network inputs, 2 neurons in the hidden layer and 1 network output with learning rate of 0.3, an iteration rate of 200,000 and momentum constant of 0.2.

Figure 16 shows the result plot between actual classification output value and the predicted classification output value for validation data set from the optimized network while Table 3 shows the final classification performance for both testing and validation data with a training performance of 98.45% and an MSE of 0.015.

The prediction results obtained showed that the ANN developed for the image abnormality classification was capable of achieving an overall accuracy of 97.5 and 92.5% for both testing and validation data, respectively, which is comparable to the

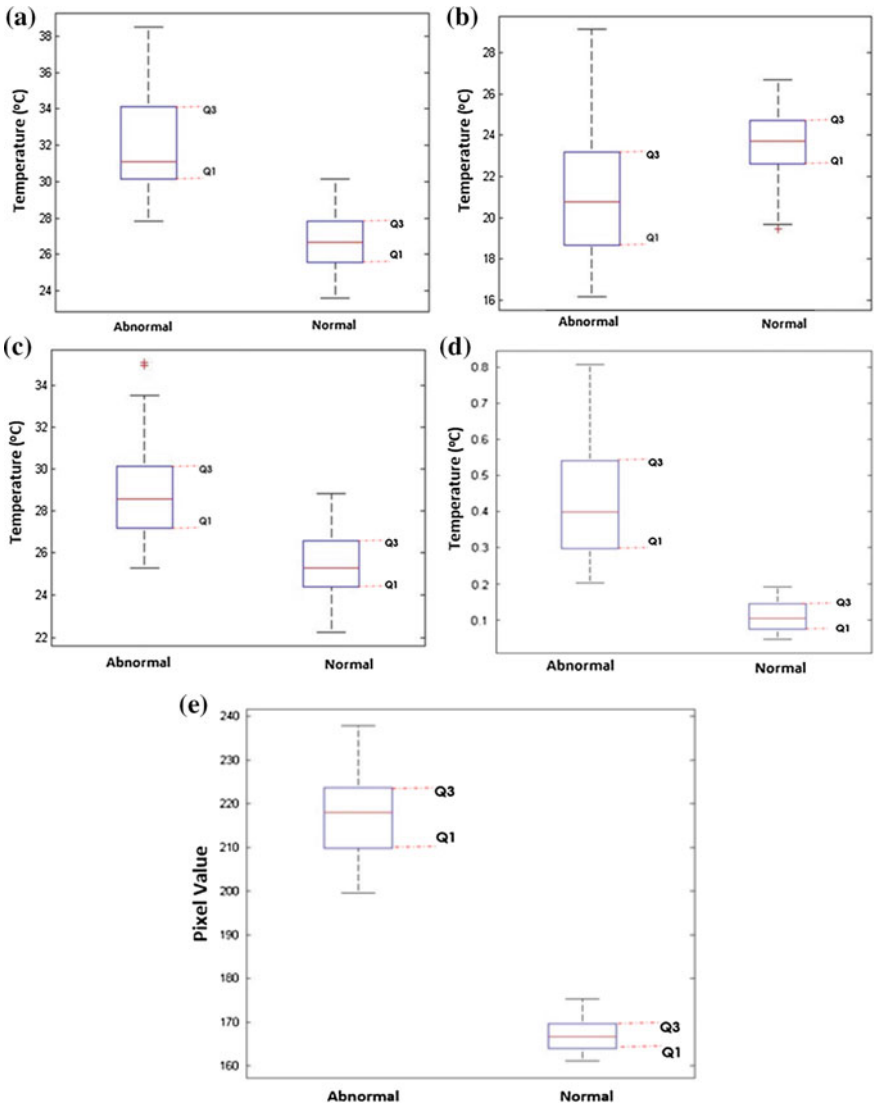

Fig. 15 Comparison of **a** maximum temperature, **b** minimum temperature, **c** mean temperature, **d** standard deviation of temperature and **e** mean intensity value for both abnormal and normal groups

performance achieved by other techniques [23, 29, 38]. This finding indicates the higher possibility of using features extracted from both visual image and temperature data in assisting clinicians to improve the current breast oncology diagnosis process.

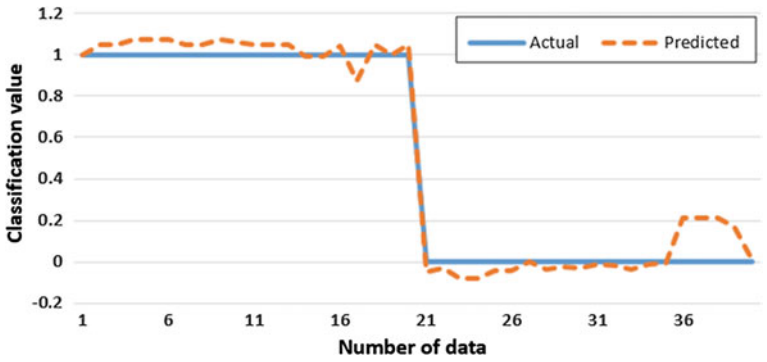

Fig. 16 Plot of actual classification value against predicted classification value for thermal image abnormality detection

Table 3 Classification results for abnormality detection

Data	Testing		Validation	
	Abnormal	Normal	Abnormal	Normal
Actual data	20	20	20	20
ANN prediction	20	19	19	18
Group accuracy (%)	100	95	95	90
Total accuracy (%)	97.5		92.5	

5 Conclusion

In this chapter, a two-tier segmentation method was proposed to automatically segment the symptomatic regions lie within the subject of interest. Features from both thermal visual image and data temperature file were extracted and fed into ANN classification system to assist the analyst in diagnosing multiple thermal images with low processing time and computational load required. A total of 200 thermal images were used to test the framework and show that the proposed method is capable in processing a large number of images from mass screening activities. This approach has produced a high accuracy of 92.5%. For future clinical study, a large data set from both healthy and cancer patients is required in both thermal visual and data temperature point formats to confirm the efficacy of this method.

Acknowledgements The authors would like to express gratitude to Universiti Teknologi Malaysia for supporting this research under the Institutional Research Grants Vote Number 05H92 and also to the Malaysian Ministry of Higher Education (MOHE) for providing the MyBrain scholarship to the author.

References

1. Saslow, D., Solomon, D., Lawson, H.W., Killackey, M., et al.: American Cancer Society, American Society for Colposcopy and Cervical Pathology, and American Society for Clinical Pathology screening guidelines for the prevention and early detection of cervical cancer. Am. J. Clin. Pathol. **137**, 516–542 (2012)
2. Canada Cancer Society, Canadian Cancer Statistics Special topic : Predictions of the future burden of cancer in Canada (2015)
3. American Cancer Society: Cancer Facts & Figures (2013)
4. Yip, C.H., Pathy, N.B., Teo, S.H.: A review of breast cancer research in Malaysia. Med. J. Malaysia **69**, 8–22 (2014)
5. Pathy, N.B., Yip, C.H., Taib, N.A., Hartman, M., et al.: Breast cancer in a multi-ethnic Asian setting: results from the Singapore-Malaysia hospital-based breast cancer registry. Breast **20** (Suppl 2), S75–S80 (2011)
6. Osako, T., Iwase, T., Takahashi, K., Iijima, K., et al.: Diagnostic mammography and ultrasonography for palpable and nonpalpable breast cancer in women aged 30 to 39 years. Breast Cancer **14**, 255–259 (2007)
7. Kavanagh, A.M., Giles, G.G., Mitchell, H., Cawson, J.N.: The sensitivity, specificity, and positive predictive value of screening mammography and symptomatic status. J. Med. Screen. **7**, 105–110 (2000)
8. Kennedy, D.A., Lee, T., Seely, D.: A comparative review of thermography as a breast cancer screening technique. Integr. Cancer Ther. **8**, 9–16 (2009)
9. Sree, S.V., Ng, E.Y.K., Acharya, R.U., Faust, O.: Breast imaging: a survey. World J. Clin. Oncol. **2**, 171–178 (2011)
10. Head, J.F., Elliott, R.L.: Infrared imaging: making progress in fulfilling its medical promise. IEEE Eng. Med. Biol. Mag. **21**, 80–85 (2002)
11. Keyserlingk, J.R., Ahlgren, P.D., Yu, E., Belliveau, N., Yassa, M.: Functional infrared imaging of the breast. IEEE Eng. Med. Biol. Mag. **19**, 3 (2000)
12. Foster, K.R.: Thermographic detection of breast cancer. IEEE Eng. Med. Biol. Mag. **17**, 6 (1998)
13. Borchartt, T.B., Conci, A., Lima, R.C.F., Resmini, R., Sanchez, A.: Breast thermography from an image processing viewpoint: a survey. Sig. Process. **93**, 2785–2803 (2013)
14. Lipari, C.A., Head, J.F.: Advanced infrared image processing for breast cancer risk assessment. In: Proceedings of 19th Annual International Conference IEEE Engineering Medical Biological Society Magnificent Milestones and Emergency Opportunities in Medical Engineering (Cat. No. 97CH36136), vol. 2, pp. 673–676 (1997)
15. Head, J.F., Wang, F., Lipari, C.A., Elliott, R.L.: The important role of infrared imaging in breast cancer. IEEE Eng. Med. Biol. Mag. **19**, 52–57 (2000)
16. Ng, E.Y.K., Fok, S.-C.: A framework for early discovery of breast tumor using thermography with artificial neural network. Breast J. **9**, 341–343 (2003)
17. Ng, E.Y.-K.: A review of thermography as promising non-invasive detection modality for breast tumor. Int. J. Therm. Sci. **48**, 849–859 (2009)
18. Herry, C.L., Frize, M.: Digital processing techniques for the assessment of pain with infrared thermal imaging. In: Proceedings of Second Joint 24th Annual Conference Annual Fall Meeting Biomedical Engineering Society [Engineering Med. Biol.], vol. 2 (2002)
19. Scales, N., Herry, C., Frize, M.: Automated image segmentation for breast analysis using infrared images. In: Conference Proceedings IEEE Engineering in Medicine and Biology Society, vol. 3, pp. 1737–1740 (2004)
20. Motta, L.S., Conci, A., Lima, R.C.F., Diniz, E.M.: Automatic segmentation on thermograms in order to aid diagnosis and 2D modeling. In: Proceedings of 10th Workshop em Informática Médica, Belo Horizonte, MG, Brazil, vol. 1, pp. 1610–1619 (2010)
21. Schaefer, G., Závišek, M., Nakashima, T.: Thermography based breast cancer analysis using statistical features and fuzzy classification. Pattern Recogn. **42**, 1133–1137 (2009)

22. Schaefer, G., Nakashima, T., Zavisek, M., Yokota, Y., et al.: Breast cancer classification using statistical features and fuzzy classification of thermograms. In: 2007 IEEE International Fuzzy System Conference (2007)
23. Ng, E.Y.K., Kee, E.C.: Advanced integrated technique in breast cancer thermography. J. Med. Eng. Technol. **32**, 103–114 (2008)
24. Ng, E.Y.K., Ung, L.N., Ng, F.C., Sim, L.S.J.: Statistical analysis of healthy and malignant breast thermography. J. Med. Eng. Technol. **25**, 253–263 (2001)
25. Acharya, U.R., Ng, E.Y.K., Tan, J.-H., Sree, S.V.: Thermography based breast cancer detection using texture features and Support Vector Machine. J. Med. Syst. **36**, 1503–1510 (2012)
26. Jones, B.F., Schaefer, G., Zhu, S.Y.: Content-based image retrieval for medical infrared images. In: Proceedings 26th Annual International Conference IEEE EMBS, pp. 1–5, San Francisco, CA, USA (2004)
27. Kuruganti, P.T., Qi, H.Q.H.: Asymmetry analysis in breast cancer detection using thermal infrared images. In: Proceedings of Second Joint 24th Annual Conference Annual Fall Meeting Biomedical Engineering Society [Engineering Med. Biol.], 2, pp. 7–8 (2002)
28. Jakubowska, T., Wiecek, B., Wysocki, M., Drews-Peszynski, C., Strzelecki, M.: Classification of breast thermal images using artificial neural networks. J. Med. Infomatics Technol. **7**, 41–50 (2004)
29. Borchartt, T.B., Resmini, R., Conci, A., Martins, A., et al.: Thermal feature analysis to aid on breast cancer diagnosis. In: Proceeding COBEM 2011, Brazil, 24–28 Oct 2011
30. Hakkak, R., Holley, A.W., Macleod, S.L., Simpson, P.M., et al.: Obesity promotes 7,12-dimethylbenz(a)anthracene-induced mammary tumor development in female zucker rats. Breast Cancer Res. **7**, R627–R633 (2005)
31. Bezerra, L.A., Oliveira, M.M., Rolim, T.L., Conci, A., et al.: Estimation of breast tumor thermal properties using infrared images. Sig. Process. **93**, 2851–2863 (2013)
32. Struck, M.B., Andrutis, K.A., Ramirez, H.E., Battles, A.H.: Effect of a short-term fast on ketamine-xylazine anesthesia in rats. J. Am. Assoc. Lab. Anim. Sci. **50**, 344–348 (2011)
33. Dice, L.R.: Measures of the amount of ecologic association between species. Ecology **26**, 297–302 (1945)
34. Jaccard, P.: La distribution de la flore dans la zone alpine. Rev. Générale des Sci. (1906)
35. Fleiss, J.L., Levin, B., Paik, M.C.: The measurement of interrater agreement. Stat. Meth. Rates Proportions **52**, 598–626 (2003)
36. Wishart, G.C., Campisi, M., Boswell, M., Chapman, D., et al.: The accuracy of digital infrared imaging for breast cancer detection in women undergoing breast biopsy. Eur. J. Surg. Oncol. **36**, 535–540 (2010)
37. Wiecek, B., Danych, R., Zwolenik, Z., Jung, A., Zube, J.: Advanced thermal image processing for medical and biological applications. In: 2001 Proceedings of 23rd Annual EMBS International Conference, pp. 2805–2807, Istanbul, Turkey, 25–28 Oct 2001
38. Etehadtavakol, M., Chandran, V., Ng, E.Y.K., Kafieh, R.: Breast cancer detection from thermal images using bispectral invariant features. Int. J. Therm. Sci. **69**, 21–36 (2013)